An Electrostatically Embedded QM/MM Scheme for Electrified Interfaces

Nawras Abidi and Stephan N. Steinmann*

Ecole Normale Supérieure de Lyon, CNRS, Laboratoire de Chimie UMR 5182, 46 allée d'Italie, F-69364, LYON, France

E-mail: stephan.steinmann@ens-lyon.fr

Phone: (+33)4 72 72 81 55

Abstract

Atomistic modelling of electrified interfaces remains a major issue for detailed insights in electrocatalysis, corrosion, electrodeposition, batteries and related devices such as pseudocapacitors. In these domains, the use of grand-canonical density functional theory (GC-DFT) in combination with implicit solvation models has become popular. GC-DFT can be conveniently applied not only to metallic surfaces, but also to semi-conducting oxides and sulfides and is, furthermore, sufficiently robust to achieve a consistent description of reaction pathways. However, the accuracy of implicit solvation models for solvation effects at interfaces is in general unknown. One promising way to overcome the limitations of implicit solvents is going towards hybrid quantum mechanical (QM)/molecular mechanics (MM) models. For capturing the electrochemical potential dependence, the key quantity is the capacitance, i.e., the relation between the surface charge and the electrochemical potential. In order to retrieve the electrochemical potential from a QM/MM hybrid scheme, an electrostatic embedding is required. Furthermore, the charge of the surface and of the solvent regions have to be strictly opposite in order to consistently simulate charge-neutral unit cells in MM

and in QM. To achieve such a QM/MM scheme, we present the implementation of electrostatic embedding in the popular VASP code. This scheme is broadly applicable to any neutral or charged solid/liquid interface. Here, we demonstrate its use in the context of GC-DFT for the hydrogen evolution reaction (HER) over a noble-metal-free electrocatalyst, MoS_2. We investigate the effect of electrostatic embedding compared to the implicit solvent model for three contrasting active sites on MoS_2: (i) the sulfur vacancy defect which is rather apolar. (ii) an Mo anti-site defect, where the active site is a surface bound highly polar OH group and (iii) a reconstructed edge site which is generally believed to be responsible for most of the catalytic activity. Our results demonstrate that electrostatic embedding leads to almost indistinguishable results compared to the implicit solvent for apolar systems, but has a significant effect on polar sites. This demonstrates the reliability of the hybrid QM/MM, electrostatically embedded solvation model for electrified interfaces.

1 Introduction

Modelling electrified interfaces is one of the central aspects to reach a detailed understanding of energy storage (batteries, pseudo-/super-capacitors) and conversion (electrolysers and fuel cells) devices, but also for corrosion and metal-deposition.[1] In the presence of a liquid electrolyte a "double layer" forms at these electrified interfaces: The surface charge is compensated by a charge distribution of the electrolyte in solution. The models for the electrochemical double layer have a long history and continue to be refined,[2,3] given that experimentally probing the nature of the double layer remains very challenging.[4]

From an atomistic modelling point of view, the ideal would be to model the entire system with explicit atoms and electrons, such that the most realistic and accurate description is reached. However, this is first limited by the available computing power (solid/liquid interfaces need $\sim$ 500 ps equilibration times for thousands of atoms) and second accounting for the electrochemical potential is not trivial, as the surface charge needs to be modulated

and the effective potential measured.[5,6]

Grand-canonical DFT (GC-DFT) has become the state-of-the-art framework to determine reaction and activation energies at electrified interfaces.[7–9] In short, the electrochemical potential is directly related to the workfunction of the system and tuned by the number of electrons. The grand-canonical energy $G(U)$ as a function of the potential is then obtained as:

$$G(U) = E(q) - \mu(q) \cdot q \tag{1}$$

where U is the electrochemical potential vs SHE, i.e., $\mu(q)$-4.44 eV, $\mu(q)$ the workfunction of the system at the given charge q and $E(q)$ the energy as obtained by the electronic structure code.

When investigating elementary pathways of electrocatalytic reactions or solvent decompositions at the solid-electrolyte interphase of batteries,[10] the best compromise between model accuracy and computational cost is reached when GC-DFT is combined with an implicit solvent and an electrolyte distribution that is described by the (modified) Poisson-Boltzmann equation.[11–13] Compared to simulations with explicit solvent and electrolyte molecules, the implicit solvent-electrolyte ensures a black-box, consistent treatment of the solvent-solute interactions, which is crucial for reaction pathways with intermediates of different sizes and polarities. Models that combine implicit solvent models for the bulk solvation effects with micro-solvation for more specific solvent effects have been successfully applied, but come with their own problems of achieving a consistent treatment along reaction pathways and as a function of the electrochemical potential.[14]

Many flavors of implicit solvent/electrolyte models have been[11,12,15] and still are[16–20] developed and applied over the years, but they all require some fitting to experimental solvation energies. Experimental solvation energies are well established for small molecules, but only a handful of numbers are available for solid/liquid interfaces. Furthermore, implicit solvent models have intrinsic limitations for capturing near-chemisorption of the solvent at the interface, as this interaction is strongly material dependent, in contrast with the more uni-

versal electrostatic and van der Waals-type of interactions encountered for molecular solutes. Instead of system-specific tuning of parameters,[21] several research groups have pushed for hybrid solvation schemes, where the (surface) reactions are described at the density functional theory (DFT) level and the solvent effects are captured by molecular mechanics (MM).[22–24] MM is many orders of magnitudes less expensive than DFT and, therefore, extensive phase-space sampling of the liquid is easily in reach. Furthermore, compared to implicit solvents, it is clearer how to improve the quality of the description of the interface energetics: Force fields can be tested against DFT and system-specifically improved.[25,26] As an example, we have shown that a purpose-built force field for the interaction of water with the Pt(111) surface[27] leads to a semi-quantitative agreement with experiment for the adsorption of phenol and benzene on Pt(111), while the standard implicit solvent gives qualitatively wrong results when comparing the adsorption in the gas-phase with adsorption form the liquid.[28] Similarly, good agreement between DFT and MM solvation energies have been achieved at the alumina/water interface.[29] Concurrently, MM is inherently able to capture entropic solvation effects, a topic that remains challenging for implicit solvent models even for small molecules.[30]

When moving from neutral surfaces to electrified (and thus charged) surfaces one faces a conceptual issue: given that the energy of a charged periodic system is infinite, the solvation energy is no longer well defined. As a result, one cannot separately compute the energy of the system at the DFT and at the MM level to obtain a hybrid QM/MM energy. Instead, what is known as an "electrostatic embedding" is necessary: The DFT computations are performed in presence of a counter-charge that is derived from the MM phase-space sampling, in analogy to the coupling between molecular and electronic DFT.[31] Electrostatic embedding for determining solvation energies has been mostly explored for neutral molecular systems.[32–34] Only very recently (and independently from us), such an approach has been applied to electrified interfaces.[35,36] Electrostatic embedding is available in most molecular DFT codes, but only rarely in plane-waves codes,[37,38] even though charged interfaces are

common, not only for electrified systems, but are also typical for oxide surfaces as a function of pH.

Here we report the implementation of electrostatic embedding in the widely used VASP code by relying on a VASPsol[18]-based interface. The electrostatic embedding is completely general, i.e., it can handle any distribution of charges from 1 to millions and neutral or charged systems. This allows us to apply GC-DFT at an approximate QM/MM level and to demonstrate the difference between the implicit solvent and the electrostatic embedding. Our results reveal that for apolar surfaces the two schemes are nearly indistinguishable, but that the electrostatic embedding stabilizes polar adsorbates significantly more compared to the implicit solvent.

2 Theoretical Background and Methods: Simplified QM/MM Solvation Energies for Charged Interfaces

An alternative to implicit solvation at the solid/liquid interface has been introduced by several groups in the form of (approximate) QM/MM schemes.[22–24] The solvation energy ΔG_{solv} as obtained by QM/MM methods is most usefully decomposed into two components:

$$\Delta G_{solv} = G_{el} + G_{non-el} \tag{2}$$

where G_{el} is the electrostatic interaction between the solvent and the solute and G_{non-el} covers the remaining, non-electrostatic, interaction free energies, most notably the Lennard-Jones interactions in the case of "standard" force fields, but also near-chemisorption terms as described by the GAL family of force fields.[25–27]

In the most straight forward (and most approximate) QM/MM scheme, ΔG_{solv} is determined exclusively at the MM level (no back polarization of the QM subsystem by the MM subsystem) of theory via free energy perturbation (FEP)[39] or thermodynamic integration

(TI).[28]

$$\Delta G_{solv}^{MMsolv} = G_{el}^{MM} + G_{non-el}^{MM} \tag{3}$$

This mechanical embedding approach, called MMsolv, has been shown to accurately capture the competition between adsorption of aromatic molecules and water on Pt(111) when compared to experiment.[28]

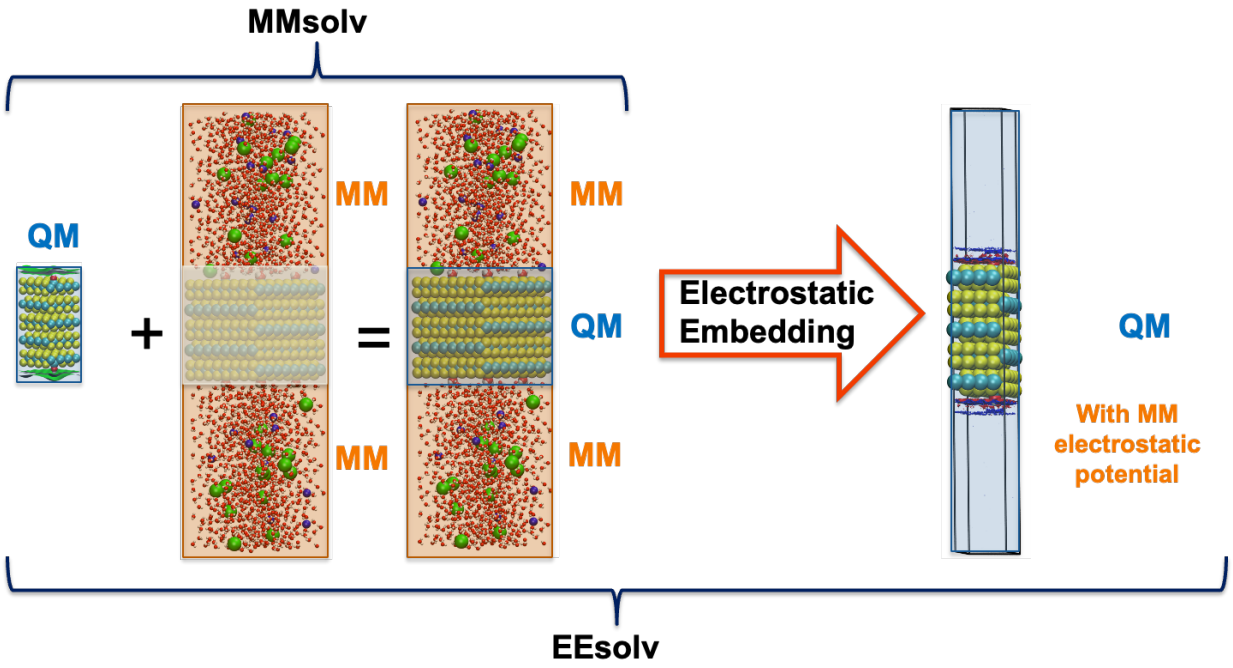

Figure 1: Schematic of our approximate QM/MM schemes. In MMsolv the QM/MM energy is a simple addition of the QM energy plus a MM-derived solvation free energy. With the electrostatic embedding (EEsolv) the charge distribution of the MM level is utilized to determine a corrected QM energy accounting for the electrostatic interaction between the two subsystems. In principle the scheme can be made self-consistent by cycling between QM and MM.

Under periodic boundary conditions the unit cells have to be neutral. Hence, computing the electrostatic solvation energy component becomes dependent on the size of the unit cell and various (approximate) corrections are required to remove the spurious contribution of the unavoidable homogeneous background charge.[40] Establishing these corrections consistently for arbitrary QM and the MM subsystems is cumbersome. As an alternative, we here evaluate G_{el} at the QM level through the embedding of the QM subsystem in the charge-distribution

of the MM subsystem (see Fig. 1). The G_{non-el} interaction is, however, still determined by FEP or TI, leading to what we call EEsolv:

$$\Delta G_{solv}^{EEsolv} = G_{el}^{QM} + G_{non-el}^{MM} \tag{4}$$

In order to assess the electrostatic interaction energy between the solvent and the solute, the solvent and electrolyte charge distribution as obtained by the sampling at the MM level needs to be included at the DFT level. In order to be compatible with the plane-wave DFT descripiton, the MM-derived point-charges are represented as sharp Gaussian charges. Since the solvent molecules undergo thermal fluctuations anyway, the technical reason for the Gaussian blur is, furthermore, physically justified in the context of solvent effects. We refer the interested reader to section S1 for the details of the freely available implementation in VASPsol and the practical aspects thereof.

3 Computational Details

All DFT computations have been performed with VASP,[41,42] linked to a (modified) version of VASPsol to enable the use of point-charges, tentatively called VASPEE. The core-electron interaction are described by the PAW formalism[43,44] using the standard pseudopotentials. The functional was chosen to be the dispersion corrected generalized gradient approximation, PBE-dDsC.[45,46] If not specified otherwise, the plane-wave cutoff was set to 500 eV, and the settings for the numerical grids were "accurate". The wavefunctions have been converged to an energy threshold below 10^{-5} eV.

All molecular dynamics (MD) simulations have been carried out by AMBER[47] and are driven by a modified version of the SolvHybrid package.[28] The geometries of the DFT subsystems are frozen during the MD runs. The water model was chosen to be TIP3P[48] and the parameters for singly-charged ions (Na^+, Cl^-) were chosen accordingly from the amber force field. If not stated otherwise, the interaction between the DFT subsystem and the MM

solvent are described by CM5 point-charges[49] combined with Lennard-Jones parameters obtained by the default combination rules as implemented in tleap, where the parameters for the DFT subsystem are taken from UFF,[50] except for MoS_2 for which more accurate parameters are available.[51] Water molecules were kept in their fixed geometry relying on the SHAKE algorithm.[52,53]

In a typical setup, the geometry is optimized at the DFT level using VASPsol (isodensity (NC_K) of 0.000250 $e^-/Å^{-1}$), up to forces below 0.05 eV/Å. The Debye screening length has been set to 3 Å, representative of a 1 M ionic strength. The atomic charges are then extracted and the system prepared via SolvHybrid for a MD run in AMBER. We generally used 2×2 supercells compared to the DFT unit cell in order to fit twice the cutoff radius (8 Å) plus the boundary layer (2 Å) inside the MM unit cell. The system is optimized for 100 steps, heated to 300 K during 200 ps, equilibrated in the NpT ensemble using the Berendsen barostat[54] for 300 ps and then a production run of 6 ns in the NVT ensemble using a Langevin thermostat is performed. For the equilibration and production runs a finer FFT (roughly two points per Å) and a larger real space cutoff (10 Å) has been used to ensure a good description of the charged interface. The charge of the surfaces was neutralized via a $\sim$ 1 M solution of NaCl. Snapshots are saved every 1 ps to obtain the charge distribution that is used for VASPEE, leading to averages over 6000 snapshots. Figure S5 and S6 provide convergence tests, showing that already 1200 snapshots would be enough to reach converged results. Furthermore, a binning of 0.25 Å leads to an acceptable accuracy, while reducing the number of charges (and thus the associated computational cost) by about 50%.

4 Results and Discussion

4.1 Solvation Energies from Electrostatic Embedding

As a first "real" example for the use of VASPEE we have computed the electrostatic components of the solvation energy of various systems, see Fig. 2. Starting with the water

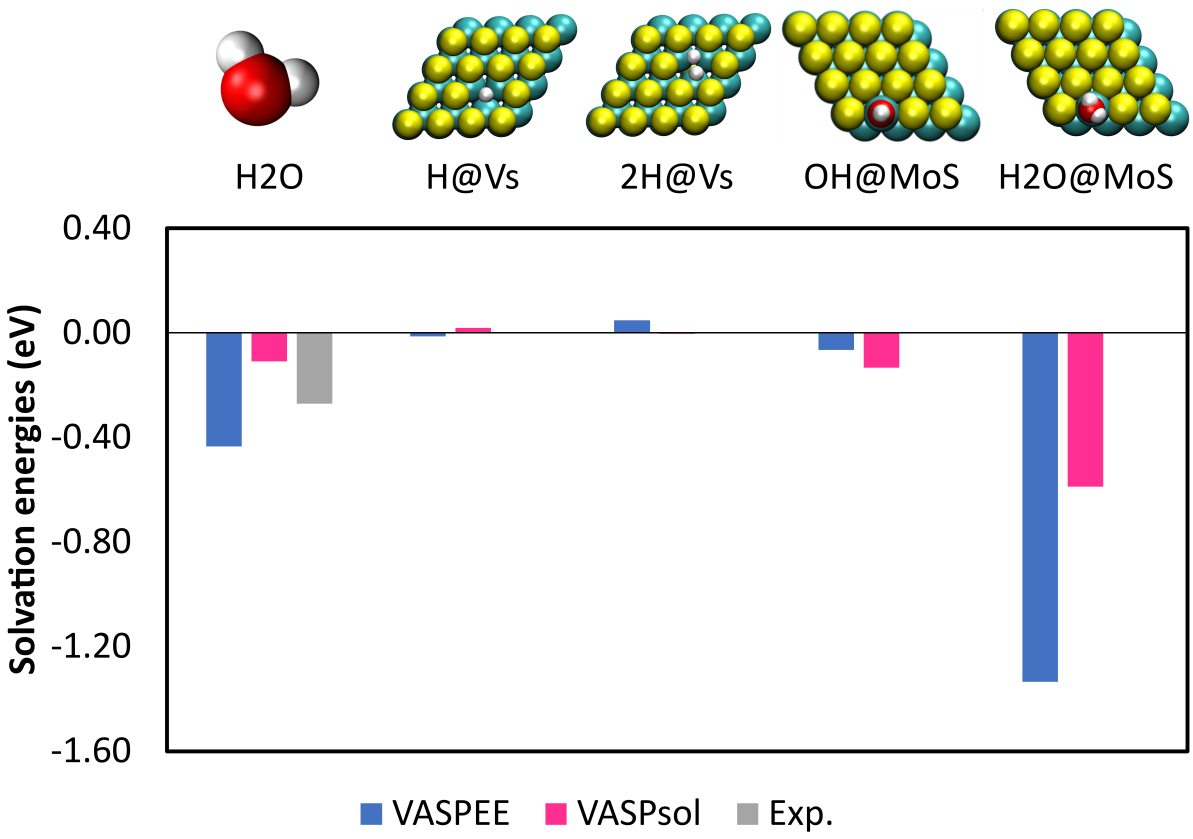

Figure 2: Electrostatic solvation energies obtained with VASPsol and EEsolv for water, two non-polar adsorbates on the sulfur vacancy on the MoS_2 basal plane and two polar adsorbates on the corresponding anti-site defect. The experimental solvation energy of water in water[49] is indicated in grey.

molecule, we observe that the adopted iso-density value for the implicit solvent (chosen to inhibit implicit solvent going between layers of MoS_2[55]) leads to an under-solvation of water -0.11 eV compared to -0.27 eV according to experiment.[49] This is expected, given that the implicit solvent has been "pushed away" from the solute by these settings. For the rather non-polar systems, exemplified by the H-covered sulfur vacancy defects (Vs), the agreement between VASPEE and VASPsol is good, suggesting that in these systems the water solvent does not play a major role. This situation changes, however, for closely related anti-site defects in MoS_2, which we have shown to be covered by OH* or H_2O*.[55] Indeed, for these quite polar systems the difference between VASPsol and VASPEE are significant, especially for H_2O*. Apparently, the chemisorbed water molecule benefits much more strongly from the solvation at the solid/water interface than the OH* adsorbate.

4.2 Grand-canonical DFT with Electrostatic Embedding

We now turn to the actual target application: The description of charged surfaces. To start with, we analyze the charge distribution on the positively charged MoS_2 OH* covered anti-site defect (see Fig. 3). It turns out the countercharge contribution is only responsible for about 1% of the total polarization density. This might explain why previous reports have suggested that achieving realistic counter-charge distributions does not merit significant efforts.[14,56] However, as can be seen from the top figure, the total charge distribution changes significantly when moving from the implicit to the explicit solvent: Not only does an MM-derived charge distribution show more fine-structure, but also the intensity of the polarization is very different. The identification of the origin of this difference in structuring is beyond the scope of the present study, but could be due to the competition between the electrostatic and the non-electrostatic interactions. If so, we would expect the difference to be even higher on metallic surfaces, where the near-chemisorption of water leads to a more structured interface.[25]

Then we analyse the grand-canonical energy as a function of the electrochemical potential.

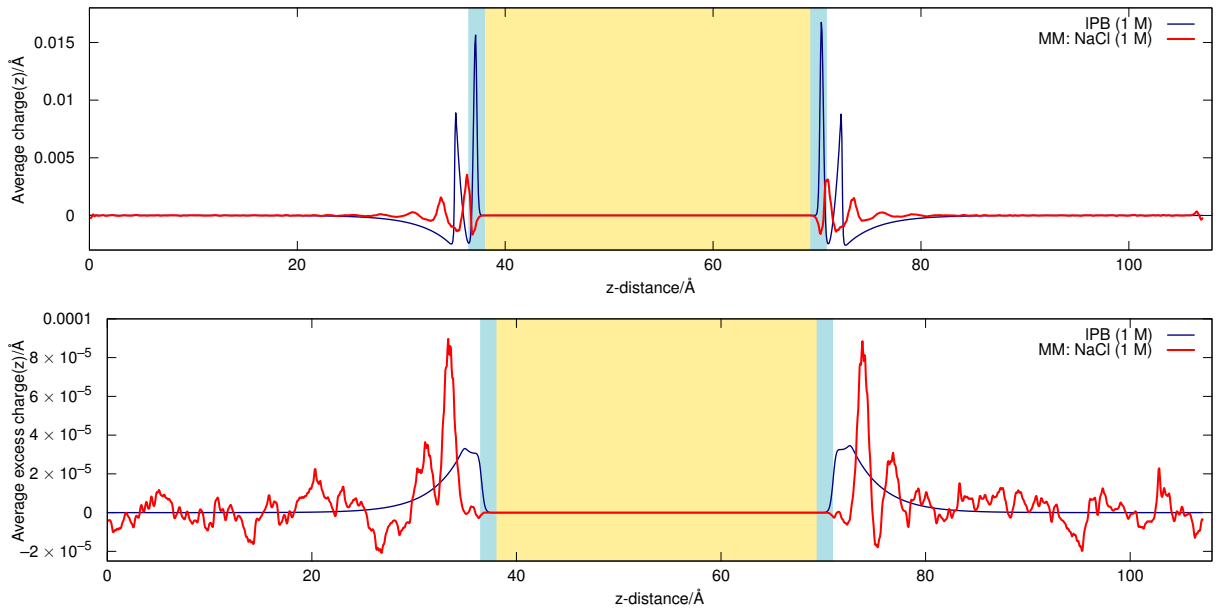

Figure 3: Average charge polarization density across the unit cell for VASPsol (lPBE) in blue and EEsolv (NaCl) in red. The top shows the total (solvent plus electrolyte), while the bottom only shows the contribution of the countercharge distribution. The yellow zones correspond to the volume occupied by MoS_2 and the blue zone indicates the location of OH*.

Still using the same model system to exemplify the effect of EEsolv, Figure 4 shows the significantly different behavior when using the implicit and the explicit solvent. The first observation is that EEsolv leads to a reasonably parabolic behavior, with the maximum being at the potential of zero charge as required for such a capacitor (see also ref[57] and discussion therein). This gives us further confidence that the scheme is working consistently across the range of charges investigated. The second observation is that towards the negative potentials (which are the ones of interest for HER) the curvature (capacitance) is very similar for VASPEE and VASPsol. In other words, the stabilization of the negative surface charge is quite well captured by the linearized Poisson-Boltzmann equation, even though the solvent is quite "far away" from the surface. However, the potential of zero charge and the capacitance for the positively charged surface differ: Indeed, the asymmetry between the positive and negative surface-charges is significantly more pronounced at the EEsolv level of theory, presumably because cations (Na^+) and anions (Cl^-) have different sizes and solvation

shells.[58]

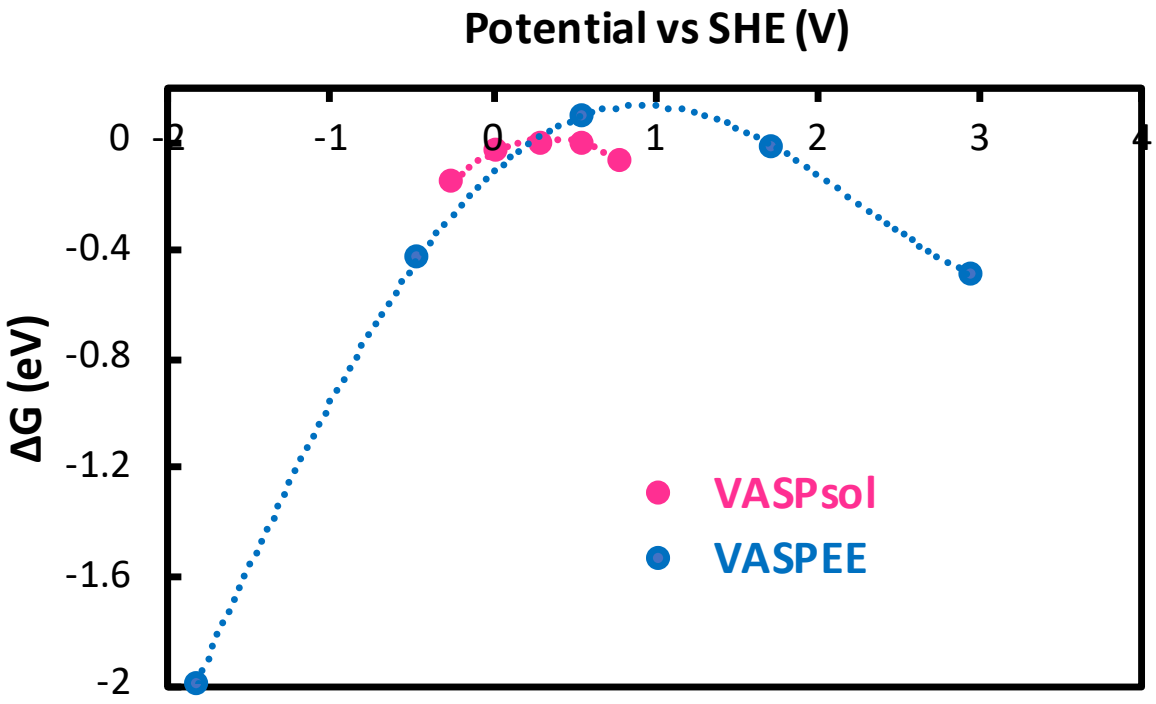

Figure 4: Grand-canonical free energy (see Eq. 1) for OH* adsorbed on the anti-site defect. The 2×2 super-cell compared to DFT has been charged with +1 and +2 electron/Na^+ pairs for the negative potentials and with -1 and -2 electron/Cl^- pairs for the positive potentials. The energy of the neutral, VASPsol-solvated surface is taken as the reference.

Now that we have gained confidence in the viability of EEsolv, we turn to the hydrogen evolution reaction. Figure 5 shows the adsorption energy as a function of the electrochemical potential of hydrogen on two potential active sites on the basal-plane of MoS_2:[55] the sulfur vacancy and the OH* covered anti-site defect. One recognizes that for the apolar active site, the two approaches coincide. In other words, the explicit and implicit solvation models solvate these geometries to a similar extent. This is in good agreement with the weak interaction of water molecules with this defect determined at the DFT level,[55] but also with the rather weakly interacting Lennard-Jones potentials.[51]

This situation changes dramatically when moving to OH* on the anti-site defect. As already seen in Fig. 2, the chemisorbed water molecule is significantly more solvated at the interface compared to OH* when using explicit solvation instead of the contiuum model. This

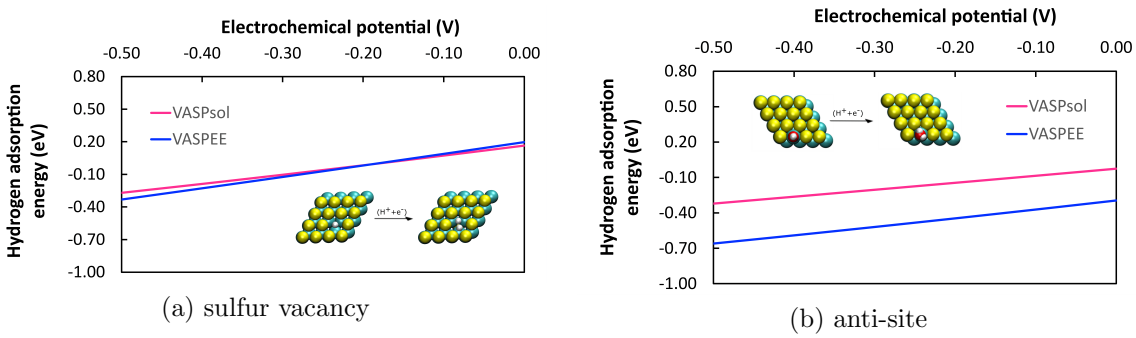

(a) sulfur vacancy

(b) anti-site

Figure 5: Adsorption energy of $H^+ + e^-$ as a function of the electrochemical potential on the sulfur vacancy (a) and the OH* covered anti-site defect (b).

increases the strength of the adsorption energy of the proton/electron pair on the active site, so that a higher thermodynamic overpotential would be required to drive HER according to EEsolv, compared to the implicit solvent (0.2 V vs 0 V, see Table S3).

According to experiments, the HER reaction over MoS_2 is dominated by active sites on the edges.[59] Previously, we have assessed the activity and stability of these edges sites by GC-DFT in combination with VASPsol.[55,60] Here, we revisit their activity with VASPEE (Figure. 6). The first active site closely resembles the one of Fig. 5b, i.e., it is a chemisorbed OH*. Again, VASPEE solvates H_2O significantly more strongly, suggesting that the Heyrovsky step (liberation of H_2) will be limiting. The thermodynamic overpotential turns out to be equivalent and low (0.1 V), leaving the conclusion of a highly active catalytic site unchanged. In contrast, the hydrogen adsorption on the "second" active site is destabilized in VASPEE compared to the implicit solvent, leading to prohibitively high thermodynamic overpotential of 0.7 V.

Having analysed four possible active sites of MoS_2, we have evidenced non-trivial differences between the implicit and QM/MM description of the solvent effects. In other words, comparing the activity of apolar and polar active sites critically depends on the description of their solvation, suggesting that QM/MM should be routinely replace the less realistic implicit solvent model.

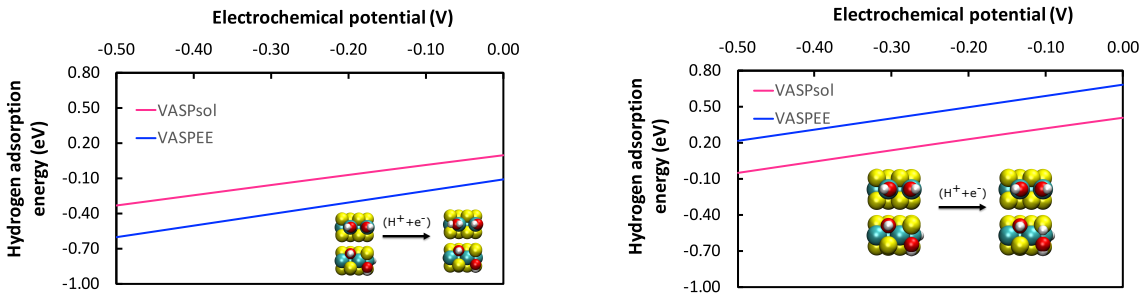

(a) Mo-edge

(b) S-edge

Figure 6: Adsorption energy of $H^+ + e^-$ as a function of the electrochemical potential on the Mo-edge covered by OH* (a) and the sulfur atom of S-edge (a).

5 Conclusion

We have implemented an electrostatic embedding for the widely used electronic structure code VASP, calling it VASPEE. The usefulness of the electrostatic embedding in VASP has been illustrated by the computation of hybrid quantum-mechanical/molecular mechanics solvation energies of solid/liquid interfaces, where the accuracy of implicit solvents is questionable. Furthermore, we have demonstrated the robustness of VASPEE and the associated sampling at the molecular mechanics level to obtain a representative solvent/electrolyte distribution at the example of two active sites of MoS_2 for the hydrogen evolution reaction. Indeed, VASPEE in combination with an Amber-based phase-space sampling allows to reach a grand-canonical DFT description of electrified interfaces with a more realistic solid/liquid interface compared to implicit solvents. For these electrified interfaces the DFT surface bears a net charge, which is exactly cancelled by the distribution of the counter-charges within the MM solvent. Analyzing the polarization density from VASPsol and VASPEE, we highlight that the major difference between the two approaches is less the electrolyte (countercharge) distribution, than the polarization of the solvent. As a consequence, VASPEE represents a cost-effective means to study solvation effects at (charged) interfaces.

Acknowledgement

This work was financially supported by Région Auvergne Rhône-Alpes through the project Pack Ambition Recherche 2018 MoSHi. The authors thank the SYSPROD project and AXELERA Pôle de Compétitivité for financial support (PSMN Data Center).

Supporting Information Available

Additional Figures and Tables containing convergence tests. The source code and two minimal working examples are also provided.

References

(1) Gonella, G.; Backus, E. H. G.; Nagata, Y.; Bonthuis, D. J.; Loche, P.; Schlaich, A.; Netz, R. R.; Kühnle, A.; McCrum, I. T.; Koper, M. T. M.; Wolf, M.; Winter, B.; Meijer, G.; Campen, R. K.; Bonn, M. Water at charged interfaces. *Nat Rev Chem* **2021**, *5*, 466–485.

(2) Baskin, A.; Prendergast, D. Exploring chemical speciation at electrified interfaces using detailed continuum models. *J. Chem. Phys.* **2019**, *150*, 041725.

(3) Huang, J.; Chen, S.; Eikerling, M. Grand-Canonical Model of Electrochemical Double Layers from a Hybrid Density–Potential Functional. *J. Chem. Theory Comput.* **2021**, *17*, 2417–2430.

(4) Favaro, M.; Jeong, B.; Ross, P. N.; Yano, J.; Hussain, Z.; Liu, Z.; Crumlin, E. J. Unravelling the electrochemical double layer by direct probing of the solid/liquid interface. *Nature Communications* **2016**, *7*, 12695.

(5) Guo, Z.; Ambrosio, F.; Chen, W.; Gono, P.; Pasquarello, A. Alignment of Redox Levels at Semiconductor–Water Interfaces. *Chem. Mater.* **2018**, *30*, 94–111.

(6) Surendralal, S.; Todorova, M.; Neugebauer, J. Impact of Water Coadsorption on the Electrode Potential of H-Pt(1 1 1)-Liquid Water Interfaces. *Phys. Rev. Lett.* **2021**, *126*, 166802.

(7) Lautar, A. K.; Hagopian, A.; Filhol, J.-S. Modeling interfacial electrochemistry: concepts and tools. *Phys. Chem. Chem. Phys.* **2020**, *22*, 10569–10580, Publisher: The Royal Society of Chemistry.

(8) Abidi, N.; Lim, K. R. G.; Seh, Z. W.; Steinmann, S. N. Atomistic modeling of electrocatalysis: Are we there yet? *WIREs Computational Molecular Science* **2021**, *11*, e1499.

(9) Abidi, N.; Steinmann, S. N. How are Transition States Modelled in Heterogeneous Electrocatalysis? *Current Opinion in Electrochemistry* **2022**, *33*, 100940.

(10) Kopač Lautar, A.; Bitenc, J.; Rejec, T.; Dominko, R.; Filhol, J.-S.; Doublet, M.-L. Electrolyte Reactivity in the Double Layer in Mg Batteries: An Interface Potential-Dependent DFT Study. *J. Am. Chem. Soc.* **2020**, *142*, 5146–5153, Publisher: American Chemical Society.

(11) Jinnouchi, R.; Anderson, A. B. Electronic structure calculations of liquid-solid interfaces: Combination of density functional theory and modified Poisson-Boltzmann theory. *Phys. Rev. B* **2008**, *77*, 245417.

(12) Wang, H.-F.; Liu, Z.-P. Formic Acid Oxidation at Pt/H2O Interface from Periodic DFT Calculations Integrated with a Continuum Solvation Model. *J. Phys. Chem. C* **2009**, *113*, 17502.

(13) Hörmann, N. G.; Andreussi, O.; Marzari, N. Grand canonical simulations of electrochemical interfaces in implicit solvation models. *J. Chem. Phys.* **2019**, *150*, 041730.

(14) Gauthier, J. A.; Dickens, C. F.; Heenen, H. H.; Vijay, S.; Ringe, S.; Chan, K. Unified Approach to Implicit and Explicit Solvent Simulations of Electrochemical Reaction Energetics. *J. Chem. Theory Comput.* **2019**, *15*, 6895–6906.

(15) Letchworth-Weaver, K.; Arias, T. A. Joint density functional theory of the electrode-electrolyte interface: Application to fixed electrode potentials, interfacial capacitances, and potentials of zero charge. *Phys. Rev. B* **2012**, *86*, 075140.

(16) Fernandez-Alvarez, V. M.; Eikerling, M. H. Interface Properties of the Partially Oxidized Pt(111) Surface Using Hybrid DFT–Solvation Models. *ACS Appl. Mater. Interfaces* **2019**, *11*, 43774–43780.

(17) Truscott, M.; Andreussi, O. Field-Aware Interfaces in Continuum Solvation. *J. Phys. Chem. B* **2019**, *123*, 3513–3524.

(18) Mathew, K.; Kolluru, V. S. C.; Mula, S.; Steinmann, S. N.; Hennig, R. G. Implicit self-consistent electrolyte model in plane-wave density-functional theory. *J. Chem. Phys.* **2019**, *151*, 234101.

(19) Ringe, S.; Hörmann, N. G.; Oberhofer, H.; Reuter, K. Implicit Solvation Methods for Catalysis at Electrified Interfaces. *Chem. Rev.* **2022**, *122*, 10777–10820.

(20) Schwarz, K.; Sundararaman, R. The electrochemical interface in first-principles calculations. *Surf. Sci. Rep.* **2020**, *75*, 100492.

(21) Bramley, G. A.; Nguyen, M.-T.; Glezakou, V.-A.; Rousseau, R.; Skylaris, C.-K. Understanding Adsorption of Organics on Pt(111) in the Aqueous Phase: Insights from DFT Based Implicit Solvent and Statistical Thermodynamics Models. *J. Chem. Theory Comput.* **2022**, *18*, 1849–1861.

(22) Saleheen, M.; Heyden, A. Liquid-Phase Modeling in Heterogeneous Catalysis. *ACS Catal.* **2018**, *8*, 2188–2194.

(23) Zhang, X.; DeFever, R. S.; Sarupria, S.; Getman, R. B. Free Energies of Catalytic Species Adsorbed to Pt(111) Surfaces under Liquid Solvent Calculated Using Classical and Quantum Approaches. *J. Chem. Inf. Model.* **2019**, *59*, 2190–2198.

(24) Steinmann, S. N.; Michel, C. How to Gain Atomistic Insights on Reactions at the Water/Solid Interface? *ACS Catal.* **2022**, *12*, 6294–6301.

(25) Steinmann, S. N.; Ferreira De Morais, R.; Götz, A. W.; Fleurat-Lessard, P.; Iannuzzi, M.; Sautet, P.; Michel, C. Force Field for Water over Pt(111): Development, Assessment, and Comparison. *J. Chem. Theory Comput.* **2018**, *14*, 3238–3251.

(26) Rey, J.; Blanck, S.; Clabaut, P.; Loehlé, S.; Steinmann, S. N.; Michel, C. Transferable Gaussian Attractive Potentials for Organic/Oxide Interfaces. *J. Phys. Chem. B* **2021**, *125*, 10843–10853.

(27) Clabaut, P.; Fleurat-Lessard, P.; Michel, C.; Steinmann, S. N. Ten Facets, One Force Field: The GAL19 Force Field for Water-Noble Metal Interfaces. *J. Chem. Theory Comput.* **2020**, *16*, 4565–4578.

(28) Clabaut, P.; Schweitzer, B.; Goetz, A. W.; Michel, C.; Steinmann, S. N. Solvation Free Energies and Adsorption Energies at the Metal/Water Interface from Hybrid Quantum-Mechanical/Molecular Mechanics Simulations. *J. Chem. Theory Comput.* **2020**, *16*, 6539 – 6549.

(29) Rey, J.; Clabaut, P.; Réocreux, R.; Steinmann, S. N.; Michel, C. Mechanistic Investigation and Free Energies of the Reactive Adsorption of Ethanol at the Alumina/Water Interface. *J. Phys. Chem. C* **2022**, *126*, 7446–7455.

(30) Garza, A. J. Solvation Entropy Made Simple. *J. Chem. Theory Comput.* **2019**, *15*, 3204–3214.

(31) Jeanmairet, G.; Levesque, M.; Borgis, D. Tackling Solvent Effects by Coupling Electronic and Molecular Density Functional Theory. *J. Chem. Theory Comput.* **2020**, *16*, 7123–7134.

(32) Fdez Galvan, I.; Sanchez, M.; Martin, M.; Olivares del Valle, F.; Aguilar, M. ASEP/MD: A program for the calculation of solvent effects combining QM/MM methods and the mean field approximation. *Computer Physics Communications* **2003**, *155*, 244–259.

(33) Lim, H.-K.; Lee, H.; Kim, H. A Seamless Grid-Based Interface for Mean-Field QM/MM Coupled with Efficient Solvation Free Energy Calculations. *Journal of Chemical Theory and Computation* **2016**, *12*, 5088–5099.

(34) González-Espinoza, C. E.; Rumble, C. A.; Borgis, D.; Wesolowski, T. A. Quantifying Fluctuations of Average Solvent Environments for Embedding Calculations. *J. Chem. Theory Comput.* **2022**, *18*, 1072–1088.

(35) Elliott, J. D.; Troisi, A.; Carbone, P. A QM/MD Coupling Method to Model the Ion-Induced Polarization of Graphene. *J. Chem. Theory Comput.* **2020**, *16*, 5253–5263.

(36) Shin, S.-J.; Kim, D. H.; Bae, G.; Ringe, S.; Choi, H.; Lim, H.-K.; Choi, C. H.; Kim, H. On the importance of the electric double layer structure in aqueous electrocatalysis. *Nat Commun* **2022**, *13*, 174.

(37) Giannozzi, P.; Andreussi, O.; Brumme, T.; Bunau, O.; Nardelli, M. B.; Calandra, M.; Car, R.; Cavazzoni, C.; Ceresoli, D.; Cococcioni, M.; Colonna, N.; Carnimeo, I.; Corso, A. D.; Gironcoli, S. d.; Delugas, P.; DiStasio, R. A.; Ferretti, A.; Floris, A.; Fratesi, G.; Fugallo, G.; Gebauer, R.; Gerstmann, U.; Giustino, F.; Gorni, T.; Jia, J.; Kawamura, M.; Ko, H.-Y.; Kokalj, A.; Küçükbenli, E.; Lazzeri, M.; Marsili, M.; Marzari, N.; Mauri, F.; Nguyen, N. L.; Nguyen, H.-V.; Otero-de-la Roza, A.; Paulatto, L.; Poncé, S.; Rocca, D.; Sabatini, R.; Santra, B.; Schlipf, M.; Seitsonen, A. P.;

Smogunov, A.; Timrov, I.; Thonhauser, T.; Umari, P.; Vast, N.; Wu, X.; Baroni, S. Advanced capabilities for materials modelling with Quantum ESPRESSO. *J. Phys.: Condens. Matter* **2017**, *29*, 465901.

(38) Olsen, J. M. H.; Bolnykh, V.; Meloni, S.; Ippoliti, E.; Bircher, M. P.; Carloni, P.; Rothlisberger, U. MiMiC: A Novel Framework for Multiscale Modeling in Computational Chemistry. *J. Chem. Theory Comput.* **2019**, *15*, 3810–3823.

(39) Steinmann, S. N.; Sautet, P.; Michel, C. Solvation free energies for periodic surfaces: comparison of implicit and explicit solvation models. *Physical Chemistry Chemical Physics* **2016**, *18*, 31850–31861.

(40) Blumberger, J.; Bernasconi, L.; Tavernelli, I.; Vuilleumier, R.; Sprik, M. Electronic Structure and Solvation of Copper and Silver Ions: A Theoretical Picture of a Model Aqueous Redox Reaction. *J. Am. Chem. Soc.* **2004**, *126*, 3928–3938.

(41) Kresse, G. Ab initio molecular dynamics for liquid metals. *Journal of Non-Crystalline Solids* **1995**, *192-193*, 222–229.

(42) Kresse, G.; Furthmüller, J. Efficient iterative schemes for *ab initio* total-energy calculations using a plane-wave basis set. *Physical Review B* **1996**, *54*, 11169–11186.

(43) Blochl, P. E. Projector augmented-wave method. **1994**, *50*, 17953.

(44) Kresse, G.; Joubert, D. From ultrasoft pseudopotentials to the projector augmented-wave method. *Physical Review B* **1999**, *59*, 1758–1775.

(45) Perdew, J. P.; Burke, K.; Ernzerhof, M. Generalized Gradient Approximation Made Simple. *Physical Review Letters* **1996**, *77*, 3865–3868.

(46) Steinmann, S. N.; Corminboeuf, C. Comprehensive Benchmarking of a Density-Dependent Dispersion Correction. *J. Chem. Theory Comput.* **2011**, *7*, 3567–3577.

(47) Case, D. A.; Cheatham, T. E.; Darden, T.; Gohlke, H.; Luo, R.; Merz, K. M.; Onufriev, A.; Simmerling, C.; Wang, B.; Woods, R. J. The Amber biomolecular simulation programs. *Journal of Computational Chemistry* **2005**, *26*, 1668–1688.

(48) Jorgensen, W. L.; Chandrasekhar, J.; Madura, J. D.; Impey, R. W.; Klein, M. L. Comparison of simple potential functions for simulating liquid water. *The Journal of Chemical Physics* **1983**, *79*, 926–935.

(49) Marenich, A. V.; Jerome, S. V.; Cramer, C. J.; Truhlar, D. G. Charge Model 5: An Extension of Hirshfeld Population Analysis for the Accurate Description of Molecular Interactions in Gaseous and Condensed Phases. *Journal of Chemical Theory and Computation* **2012**, *8*, 527–541.

(50) Rappe, A. K.; Casewit, C. J.; Colwell, K. S.; Goddard, W. A.; Skiff, W. M. UFF, a full periodic table force field for molecular mechanics and molecular dynamics simulations. *Journal of the American Chemical Society* **1992**, *114*, 10024–10035.

(51) Sresht, V.; Govind Rajan, A.; Bordes, E.; Strano, M. S.; Padua, A. A.; Blankschtein, D. Quantitative modeling of MoS2–solvent interfaces: predicting contact angles and exfoliation performance using molecular dynamics. *The Journal of Physical Chemistry C* **2017**, *121*, 9022–9031.

(52) Ryckaert, J.-P.; Ciccotti, G.; Berendsen, H. J. Numerical integration of the cartesian equations of motion of a system with constraints: molecular dynamics of n-alkanes. *Journal of Computational Physics* **1977**, *23*, 327–341.

(53) Ryckaert, J. Special geometrical constraints in the molecular dynamics of chain molecules. *Molecular Physics* **1985**, *55*, 549–556.

(54) Berendsen, H. J. C.; Postma, J. P. M.; van Gunsteren, W. F.; DiNola, A.; Haak, J. R. Molecular dynamics with coupling to an external bath. *The Journal of Chemical Physics* **1984**, *81*, 3684–3690.

(55) Abidi, N.; Bonduelle-Skrzypczak, A.; Steinmann, S. N. Revisiting the Active Sites at the MoS2/H2O Interface via Grand-Canonical DFT: The Role of Water Dissociation. *ACS applied materials & interfaces* **2020**, *12*, 31401–31410.

(56) Hagopian, A.; Doublet, M.-L.; Filhol, J.-S.; Binninger, T. Advancement of the Homogeneous Background Method for the Computational Simulation of Electrochemical Interfaces. *J. Chem. Theory Comput.* **2022**, *18*, 1883–1893.

(57) Wei, Z.; Göltl, F.; Steinmann, S. N.; Sautet, P. Modeling Electrochemical Processes with Grand Canonical Treatment of Many-Body Perturbation Theory. *J. Phys. Chem. Lett.* **2022**, *13*, 6079–6084.

(58) Staub, R.; Steinmann, S. N. Parameter-free coordination numbers for solutions and interfaces. *J. Chem. Phys.* **2020**, *152*, 024124.

(59) Jaramillo, T. F.; Jørgensen, K. P.; Bonde, J.; Nielsen, J. H.; Horch, S.; Chorkendorff, I. Identification of active edge sites for electrochemical H2 evolution from MoS2 nanocatalysts. *science* **2007**, *317*, 100–102.

(60) Abidi, N.; Bonduelle-Skrzypczak, A.; Steinmann, S. N. How Stable Are 2H-MoS2 Edges under Hydrogen Evolution Reaction Conditions? *J. Phys. Chem. C* **2021**, *125*, 17058–17067.

Graphical TOC Entry